Multiphysical Lithium-Based Battery Model for Use in State-of-Charge Determination

Nicolas Watrin, *Student Member, IEEE*, Robin Roche, *Student Member, IEEE*, Hugues Ostermann, Benjamin Blunier, and Abdellatif Miraoui, *Senior Member, IEEE*

***Abstract*—This paper presents a multiphysical battery pack model, along with a procedure to identify its parameters and its application to state-of-charge (SOC) determination using an extended Kalman filter (EKF). The model enables the reproduction of the electric and thermal behaviors of batteries with high accuracy. A methodology is proposed to identify the parameters of the model and optimize them. The model is experimentally validated with measurements run on high-energy-density ThunderSky cells. A comparison of measurements and model results shows that the electrical model error is below 1.6% and that the error of the thermal model is below 2.5%. The model is used as an EKF basis to reliably estimate the battery SOC. The results are also experimentally verified through measurements showing that the proposed model performs better than other simpler models and determination methods.**

***Index Terms*—Kalman filter, lithium-ion battery, multiphysical modeling, parameter identification, state-of-charge (SOC) determination.**

I. Introduction

TO TRY to reduce the effects of global warming, the use of vehicles powered by internal combustion engines (ICEs) is expected to decrease and be replaced by hybrid electric vehicles (EVs), in which a battery enables reducing the size of the ICE and its corresponding emissions. As a consequence, over the last few years, the automotive industry has focused some of its research efforts on electrochemical storage for EVs and hybrid EVs (HEVs).

Lithium-based batteries have emerged as one of the most promising technologies for this application. These batteries can have a high energy density of more than 150 Wh/kg for high-energy cells and a high power density of more than 200 W/kg for high-power cells [1] and are thus well suited for powertrain needs. However, the electrical behavior of these batteries is hard to predict and is highly dependent on the materials used for the electrolyte and the electrodes. Moreover, having reliable information on quantities such as state-of-charge (SOC) and state-of-health (SOH), which are not directly measurable, is a requirement for operating battery-based hybrid and electric vehicles in a safe and efficient manner.

Models have been developed to tackle these issues, which is critical in the advent of the massive commercialization of these vehicles. Models are indeed required for running reliable simulations involving energy storage, e.g., for sizing powertrain components or developing energy management algorithms. One of the difficulties in the development of such models is defining an optimal tradeoff between their generic nature and their accuracy for specific batteries.

However, as many characteristics (SOC, temperature, current, etc.) of batteries are interdependent, such models tend to be rather complex. Batteries are electrochemical energy storage means that can undergo strong temperature stress, resulting from both environment (such as low winter temperatures) and use (such as long high-demand profiles). Due to these intrinsic interactions among electrical, chemical, and thermal behaviors, multiphysical models are required for studying such batteries with a satisfactory degree of accuracy.

Battery models can also be useful to determine the SOC of the battery of a vehicle, which is an equivalent of the fuel gauge of ICE-based vehicles. Contrary to the fuel level, which can be easily measured in the fuel tank [2], the energy contained at a given time in a battery is not directly accessible [3], [4]. In a lithium-ion battery, the SOC is dependent on many parameters such as temperature, current, and cycling. Estimating the SOC is thus a difficult task, particularly as it has to be done online in a hybrid electric vehicle, which *de facto* excludes voltage-based techniques. SOC estimation algorithms, based on combined current and voltage measurements such as the algorithm presented in this paper, are thus implemented on battery management systems (BMSs). This helps improve battery life duration [5]–[7] and ensure their safe operation, which could, for example, be threatened if the SOC went under or above the given limits.

This paper proposes a multiphysical model of lithium-based batteries for use in automotive applications, which is a methodology to determine its parameters and an experimental validation using a test bench. It also presents its application to SOC determination through an extended Kalman filter (EKF), which is also validated through experimental measurements.

Manuscript received December 9, 2011; revised April 19, 2012; accepted June 7, 2012. Date of publication June 18, 2012; date of current version October 12, 2012. The review of this paper was coordinated by Prof. M. Krishnamurthy.

N. Watrin is with Segula Technologie Automotive, 59491 Villeneuve d'Ascq, France (e-mail: nicolas.watrin@utbm.fr).

R. Roche and H. Ostermann are with the Research Institute on Transportation, Energy and Society, Université de Technologie de Belfort–Montbéliard, 90010 Belfort, France (e-mail: robin.roche@utbm.fr; hugues.ostermann@utbm.fr).

B. Blunier, deceased, was with the Research Institute on Transportation, Energy and Society, Université de Technologie de Belfort–Montbéliard, 90010 Belfort, France.

A. Miraoui is with the Research Institute on Transportation, Energy and Society, Université de Technologie de Belfort–Montbéliard, 90010 Belfort, France, and also with Cadi Ayyad University, Marrakesh 40000, Morocco (e-mail: abdellatif.miraoui@utbm.fr).

Color versions of one or more of the figures in this paper are available online at http://ieeexplore.ieee.org.

Digital Object Identifier 10.1109/TVT.2012.2205169

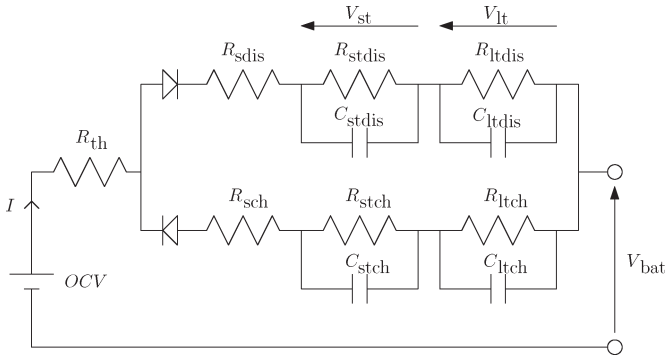

Fig. 1. Proposed electrical equivalent circuit model of a battery cell. The *dis* index is used for discharge, and *ch* is used for charge.

II. Multiphysical Battery Model

The three main categories of battery models can be identified in the literature. The first category corresponds to mathematical models [8], which are usually empirical, do not give direct relationships between phenomena [9], and are sometimes inaccurate in predicting the SOC for variable currents [10]. Very detailed electrochemical models belong to the second category and can have better accuracy but are also generally a much more computation intensive [10]–[12] and require specific battery chemical inputs. Finally, models from the last category are equivalent circuit models and can be built with several degrees of complexity, depending on the desired accuracy [13], [14]. The nonmeasurable parameters of these models can change with measurable quantities such as temperature, current, and use history [1], [11].

A. Selected Model

In this paper, the proposed model belongs to the last category and consists of an electrical equivalent circuit for each cell of the battery. This structure enables to easily adapt the accuracy of the model according to the application while maintaining a certain level of genericity, in the perspective of its use with other types of batteries. The equivalent circuit in Fig. 1 includes a resistance depending on temperature and another resistance depending on mostly SOC and two *RC* branches. I is the current, $V_{\rm bat}$ is the battery measured voltage, and OCV is the open-circuit voltage. Although the model was developed for a single cell, it can easily be extended for several cells connected in series.

B. Electrical Parameters

The proposed model contains 11 internal parameters corresponding to resistances and capacitors [11], [15].

1) Series resistance $R_{\rm th}$ represents the influence of temperature on cell impedance.
2) Series resistance R_s represents the ohmic losses related to the physical nature of the electrodes and the electrolyte.
3) The $R_{\rm st}C_{\rm st}$ branch represents the effects of the double-layer capacity, which also corresponds to the shortest time constant of the model.
4) The $R_{\rm lt}C_{\rm lt}$ branch represents the diffusion phenomenon in the electrolyte and corresponds to the slow (long) branch having the highest time constant of the model.

Each of the previous electrical parameters, except $R_{\rm th}$, is defined for both charge and discharge currents, thus increasing the number of electrical parameters from 6 to 11, to reflect the changing behavior of the cells for each case. This distinction results from the materials used on each electrode, which imply a different electrical behavior for charge and discharge, and account for the effects of hysteresis.

C. Battery Voltage

From Fig. 1, the equations governing the cell output voltage for discharge are given by

$$V_{\rm bat} = \text{OCV} - (R_{\rm th} + R_{\rm sdis}) \cdot I - V_{\rm stdis} - V_{\rm ltdis} \tag{1}$$

$$\frac{dV_{\rm stdis}}{dt} = -\frac{V_{\rm stdis}}{R_{\rm stdis}C_{\rm stdis}} + \frac{I}{C_{\rm stdis}} \tag{2}$$

$$\frac{dV_{\rm ltdis}}{dt} = -\frac{V_{\rm ltdis}}{R_{\rm ltdis}C_{\rm ltdis}} + \frac{I}{C_{\rm ltdis}}. \tag{3}$$

Solving first-order differential equation (2) gives

$$V_{\rm stdis}(t) = C \cdot \exp(a \cdot t)) - \frac{b}{a} \tag{4}$$

$$= C \cdot \exp\left(\frac{-1}{R_{\rm stdis} \cdot C_{\rm stdis}} \cdot t\right) - \frac{\frac{I}{C_{\rm stdis}}}{-\frac{1}{R_{\rm stdis} \cdot C_{\rm stdis}}} \tag{5}$$

where C is a constant that is determined using initial conditions. Initially, no current is extracted from the cell, and therefore, there is no voltage drop and $V_{\rm stdis}(0) = 0$. Initial conditions thus imply

$$V_{\rm stdis}(t) = 0 = C \cdot \exp(0) - R_{\rm stdis} \cdot I(t). \tag{6}$$

Consequently, $C = R_{\rm stdis} \cdot I$. From this, (5) can be rewritten as

$$V_{\rm stdis}(t) = R_{\rm stdis} \cdot I(t) \cdot \left[1 - \exp\left(\frac{\Delta t}{R_{\rm stdis} \cdot C_{\rm stdis}}\right)\right]. \tag{7}$$

The same method is used to solve (3), which gives

$$V_{\rm ltdis}(t) = R_{\rm ltdis} \cdot I(t) \cdot \left[1 - \exp\left(\frac{\Delta t}{R_{\rm ltdis} \cdot C_{\rm ltdis}}\right)\right]. \tag{8}$$

From (1), (7), and (8), an expression of $V_{\rm bat}$ only using determinable parameters is then derived as

$$\begin{aligned} V_{\rm bat}(t) = {} & \text{OCV} - (R_{\rm th} + R_{\rm sdis}) \cdot I(t) \\ & - R_{\rm stdis} \cdot I(t) \cdot \left[1 - \exp\left(\frac{\Delta t}{R_{\rm stdis} \cdot C_{\rm stdis}}\right)\right] \\ & - R_{\rm ltdis} \cdot I(t) \cdot \left[1 - \exp\left(\frac{\Delta t}{R_{\rm ltdis} \cdot C_{\rm ltdis}}\right)\right]. \end{aligned} \tag{9}$$

A similar expression is obtained for charge, with the corresponding parameters.

D. Temperature

Temperature has a strong influence on many battery parameters and is a crucial element to take into account for automotive applications, particularly for safety reasons. In this model, temperature is derived from the internal energy balance of the battery that accounts for losses. A large part of the losses are resistive and can be easily computed based on battery current and internal resistance values.

The total energy balance is given by

$$m \cdot C_p \cdot \frac{dT}{dt} = \sum_j \dot{Q}_j \tag{10}$$

$$= P_{\text{loss,s}} + P_{\text{loss,st}} + P_{\text{loss,lt}} - \dot{Q}_{\text{amb}} \tag{11}$$

where m stands for the mass of the cell, C_p is its specific heat, T is its temperature, and $\dot{Q}_j$ is the thermal power. This power can be positive (e.g., for Joule losses) or negative (e.g., for dissipations in the environment). These dissipations $\dot{Q}_{\text{amb}}$ can be split into three contributions, i.e., conduction, natural or forced convection, and radiation. As cells are sufficiently spaced and are not water-cooled, the conduction flux is neglected.

The radiation flux is given by

$$\dot{Q}_{\text{rad}} = \sigma \cdot \epsilon \cdot \left(T_{\text{a}}^4 - T^4\right) \tag{12}$$

where T_{a} is the ambient temperature, σ is the Stefan-Boltzmann constant, and ϵ is the cell emissivity.

The convection flux is described by

$$\dot{Q}_{\text{conv}} = h_c \cdot A \cdot (T_{\text{a}} - T) \tag{13}$$

where h_c is the cell heat transfer coefficient in $\text{W} \cdot \text{m}^{-2} \cdot \text{K}^{-1}$, and A is the cell external surface area in m^2.

During cell discharge, the energy balance in (11) can then be rewritten as a discrete system

$$\begin{aligned} m \cdot C_p \cdot \frac{T(t) - T(t-1)}{\Delta t} &= R_{\text{s}} \cdot I(t)^2 \\ &+ \frac{1}{R_{\text{stch}}} \left[\text{OCV}(t) - V_{\text{bat}}(t) - V_{\text{ltch}} - R_s \cdot I(t)\right]^2 \\ &+ \frac{1}{R_{\text{ltch}}} \left[\text{OCV}(t) - V_{\text{bat}}(t) - V_{\text{stch}} - R_s \cdot I(t)\right]^2 \\ &- \sigma \cdot \epsilon \cdot \left(T_{\text{a}}^4 - T(t)^4\right) \\ &- h_c \cdot A \cdot \left(T_{\text{a}} - T(t)\right). \end{aligned} \tag{14}$$

Solving (14) for $T(t)$ gives the temperature of the cell according to the model.

III. Model Parameter Identification

The parameters listed earlier need to be numerically identified for the model to be usable. Their identification is carried out using a pack of ten cells connected in series. Working on a model of several cells helps mitigate the importance of specific phenomena occurring in a single cell, as even two identical cells from the same manufacturer have nonidentical characteristics.

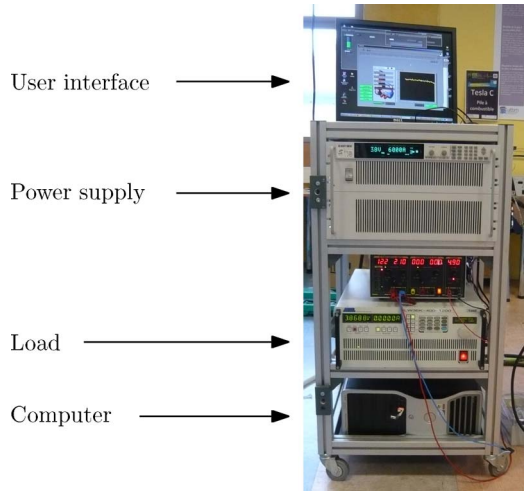

Fig. 2. Battery test bench.

A. Experimental Setup

The identification method relies on measurements run using a battery test bench.

1) Test Bench Design: The bench consists of a 36-kW dc electronic load, a 12-kW dc power supply, the tested battery pack, and a switch that activates either the power supply for charging the pack or the load for discharging it (see Fig. 2).

2) Current Profiles and Measurements: Predefined current profiles are run with the test bench through a LabView interface on a personal computer, which controls the load and the power supply and acquires measurements for the pack.

3) Cell Characteristics: The cells selected for validating the model are LFP60 LiFePO_4 cells from manufacturer Thunder-Sky, with a nominal voltage of 3.2 V and a rated capacity of 60 Ah. The maximum charge and discharge current is limited to 3C and to 20C for short impulses.

4) Safety Measures: The cutoff low voltage of each cell is set to 2.5 V, and the cutoff over voltage to 4.25 V. This avoids degrading the cells if their SOC exceeds its operational boundaries.

5) Capacity Determination: The real capacity of the cells is determined with a full discharge at a constant current of 1C. The total energy contained in each cell is obtained by multiplying the current value with the duration required to empty the cell. Measures show that the real capacity of cells differs from as much as 20% from their rated value: C_{b} was measured as equal to 71.6 Ah for each one, with changes lower than 0.1 Ah from one cell to the other. This value is thus used as the rated capacity in the following:

6) SOC Determination: To obtain a reliable value for the SOC, each determination is done using the Coulomb-counting method (15) in controlled conditions, with a constant current (1C) and temperature, i.e.,

$$\text{SOC}(t) = \text{SOC}_0 + \frac{1}{C_{\text{b}}} \int_{t=0}^{T} I(t)\, dt. \tag{15}$$

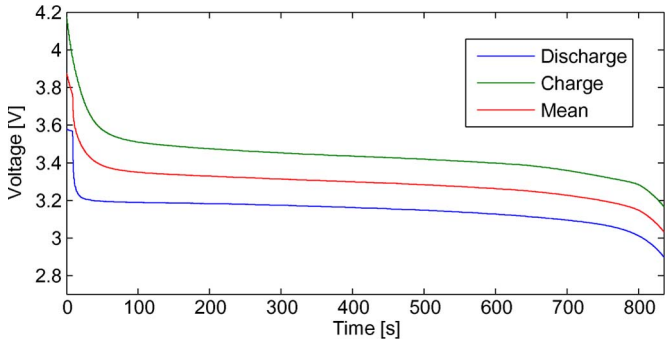

Fig. 3. Values of the OCV for charge and discharge.

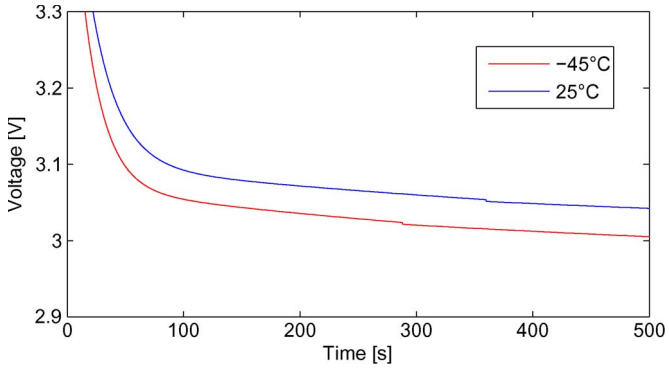

Fig. 4. Voltage profile of a cell subject to a constant current for several temperatures.

7) OCV Curves: The OCV of the cells cannot be directly determined because of the hysteresis effect. The cells are at first discharged with a constant current of 1C. The discharge is stopped at regular intervals, enabling the relaxation of the voltage, which is then measured. After a full discharge, the same method is used to obtain the OCV during charge. The final OCV (see Fig. 3) is taken as the average between the measures obtained during charge and discharge [16].

B. Initial Identification Procedure

Each parameter of the model is identified according to a different procedure, depending on what influences it (SOC, temperature, etc.).

1) Thermal Resistance: The value of $R_{\rm th}$, contrary to other parameters, only depends on temperature. It thus represents the impact of temperature on the voltage response of cells. Fig. 4 shows that the voltage profile of the same cell at the same SOC under 25 °C and −45 °C is different: the voltage drops for lower temperatures.

Knowing the current applied to the cell, the value of $R_{\rm th}$ can be derived using Ohm's law as in (16), where $\Delta V_{\rm th}$ is the voltage drop that is extracted for several SOC values from the manufacturer's data sheet. The value of the resistance is then interpolated for each temperature (see Fig. 5)

$$R_{\rm th} = \frac{\Delta V_{\rm th}}{I}. \tag{16}$$

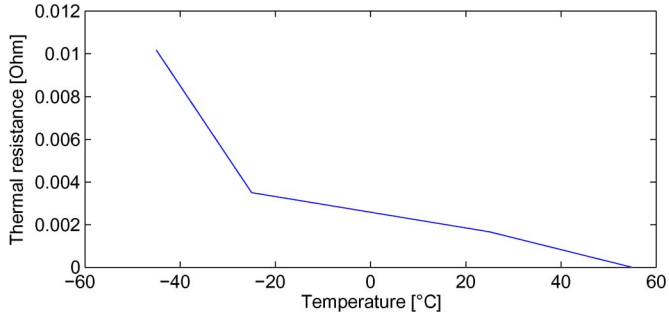

Fig. 5. Values of $R_{\rm th}$ for several temperatures.

2) Physical Parameters: For the thermal model to be usable, physical parameters such as ϵ and h_c from (14) are estimated due to manufacturer data and room conditions at the time of the test. ϵ represents the cell emissivity and depends on the material used in cell packaging. h_c represents the cell heat transfer and is deduced from the used cooling system. In this paper, no cooling system is used, which implies a low h_c value between 2 and 20 $\mathrm{W \cdot m^{-2} \cdot K^{-1}}$. In the present case, the value of h_c was initialized to 10 $\mathrm{W \cdot m^{-2} \cdot K^{-1}}$.

3) Internal Parameters: All other internal component values are dependent on the value of the current SOC. These parameter are thus defined by the following equations [12], where $i \in \{_{\rm ltdis;stdis;sdis;ltch;stch;sch}\}$:

$$R_i = a_i \cdot e^{(b_i \cdot \mathrm{SOC})} + c_i \cdot e^{(d_i \cdot \mathrm{SOC})} \tag{17}$$
$$C_i = \alpha_i \cdot e^{(\beta_i \cdot \mathrm{SOC})} + \gamma_i \cdot e^{(\delta_i \cdot \mathrm{SOC})}. \tag{18}$$

Capacitance $C_{\rm stch}$ differently evolves with SOC [17] and is given by

$$C_{\rm stch} = e \cdot \mathrm{SOC}^2 + f \cdot \mathrm{SOC} + g. \tag{19}$$

The algorithm determines the four parameters of $R_{\rm ltdis}$, $C_{\rm ltdis}$, $R_{\rm stdis}$, $C_{\rm stdis}$, $R_{\rm sdis}$, $R_{\rm ltch}$, $C_{\rm ltch}$, $R_{\rm stch}$, $R_{\rm sch}$, and the three parameters of $C_{\rm stch}$. A total of 39 parameters, i.e., a_i, b_i, c_i, d_i, e, f, g, α_i, β_i, γ_i, and δ_i, thus need to be determined by the identification algorithm.

The values of the parameters are extracted from measurements by analyzing the behavior of the battery after a current step of amplitude I is applied to it. The amplitude and duration of the step is selected as low as possible so that the SOC change can be neglected.

The procedure falls into several parts.

1) At first, the cell is fully charged.
2) A current step of 1C is applied to it (see Fig. 6).
3) Based on the voltage response to this step, the parameters of the model are identified, as described in the next paragraph.
4) A current step of 0.5 C is applied to the battery.
5) The battery is discharged of 5% SOC.
6) The process goes on until the lower SOC limit is reached and is done again for charge.

The parameters of the electrical model are identified as follows:

1) Identical current steps are applied on the pack at several SOC values for both charge and discharge.

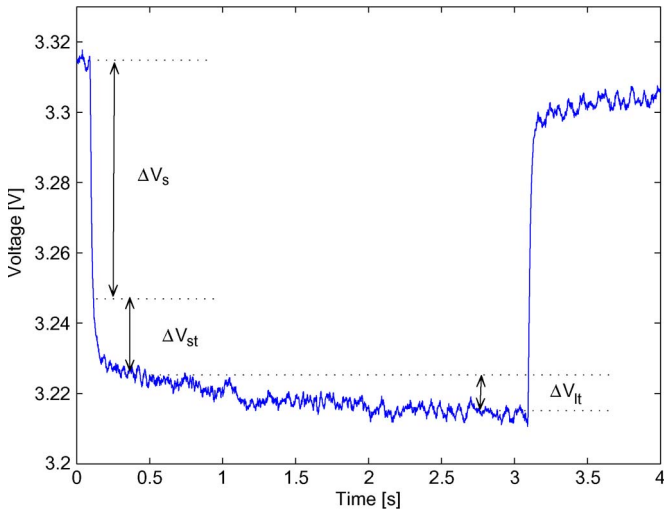

Fig. 6. Measured voltage profile of a cell after a current step used for identifying the parameters of the model.

2) Electrical parameters R_i and C_i are extracted from the obtained measurements by analyzing the voltage response of the cells to this step (see Fig. 6). The extraction of the electrical parameters is done using the following procedure:
   a) Series resistance R_s is computed as the ratio of the voltage drop V_s directly after the current step and the current step amplitude, i.e.,

$$R_{\rm s} = \frac{\Delta V_{\rm s}}{I}. \tag{20}$$

   b) The time constant of the fast transient $\tau_{\rm st}$ is obtained for one third of the fast transient voltage drop $V_{\rm st}$.
   c) The short transient resistance $R_{\rm st}$ is obtained from the voltage drop $V_{\rm st}$ during five $\tau_{\rm st}$, i.e.,

$$R_{\rm st} = \frac{\Delta V_{\rm st}}{I}. \tag{21}$$

   d) $C_{\rm st}$ is then derived from the two previous values, i.e.,

$$C_{st}\frac{\tau_{\rm st}}{R_{\rm st}}. \tag{22}$$

   e) The duration of the long transient $\tau_{\rm lt}$ is equal to one fifth of the duration of the total voltage drop between $\tau_{\rm st}$ and 1.5 s and is usually close to several hundred millisecond.
   f) The same method as earlier is applied to obtain $R_{\rm lt}$ and $C_{\rm lt}$, i.e.,

$$R_{\rm lt} = \frac{\Delta V_{\rm lt}}{I} \tag{23}$$

$$C_{\rm lt} = \frac{\tau_{\rm lt}}{R_{\rm lt}}. \tag{24}$$

3) The obtained curves $R_i(\mathrm{SOC})$ and $C_i(\mathrm{SOC})$ are then fitted using second-order exponential or polynomial fits, as in (17)–(19).

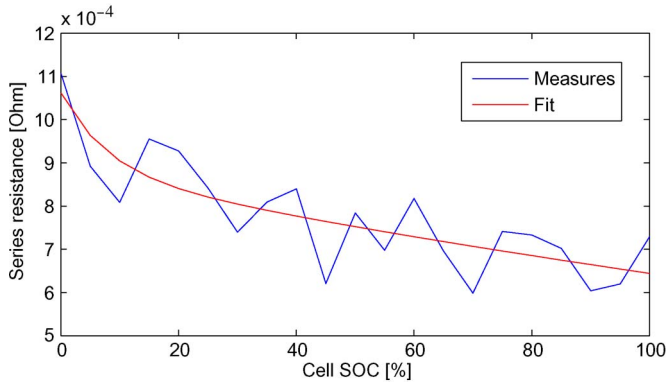

Fig. 7. Values of $R_{\rm sch}$ as a function of the SOC.

4) The parameters of these fits correspond to the searched parameters.

Once this initial determination procedure has been completed, the values of all 39 parameters of the model have been identified. Fig. 7 shows, for example, the evolution of the value of the series resistance R_s of a cell with its SOC. Although experimental values tend to have a nonmonotonic behavior, the fitted curve adequately reproduces the trend in their evolution.

C. Initial Results Optimization

Although these initial values are assumed to be rather close to their real values, they may still be improved to correct the inaccuracies of their determination process and, hereby, further improve model accuracy. This is achieved with an optimization algorithm that tries to minimize the root-mean-square (RMS) error (as in (25), shown below, where X is a vector of parameters) between the results of the model with the initial parameters and the measurements by iteratively modifying the values of the parameters. The optimization is run with Matlab's optimization algorithms on a maximum of 5000 iterations. A long and dynamic cycle is selected for this process, so that all 39 parameters can be improved, i.e.,

$$\min_X J = \sqrt{\frac{1}{N}\sum_{t=0}^{N-1}\left(V_{\rm model}(t,X) - V_{\rm meas}(t)\right)^2}. \tag{25}$$

D. Experimental Validation

After the parameters have been determined and optimized, it is necessary to compare the global model to the real battery pack to validate it.

1) Electric Model: Dynamic simulations are carried out using several intensive driving cycles. Fig. 8(a) and (b) shows the model and the measured voltage for the same cycle for the model with one and two *RC* cells.

Table I compares the RMS error (RMSE) for several sets of model parameters: initial and optimized parameters, as described earlier with two *RC* cells, and the same for a model

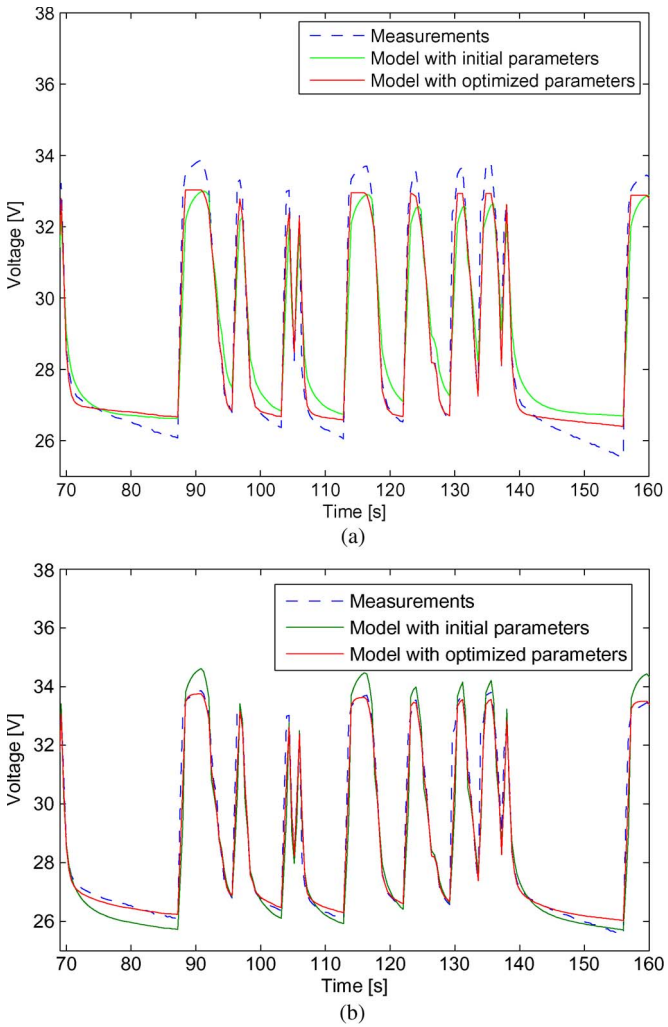

Fig. 8. Comparison of the voltage profiles obtained through measurements: a model with one and two *RC* branches and initial and optimized parameters. (a) Voltage profiles with one *RC* branch. (b) Voltage profiles with two *RC* branches.

TABLE I
COMPARISON OF MODEL PERFORMANCE FOR SEVERAL PARAMETER SETS

Set of parameters	RMS error	Max error (V)	Mean error (%)
1 RC initial	0.8964	6.2	3.2
1 RC optimized	0.4364	4.9	1.6
2 RC initial	0.6038	5.9	2.1
2 RC optimized	0.4016	4.8	1.6

with only the *RC* cell for fast transients. Results show that, as expected, adding a second *RC* cell enables improving the accuracy of the model when the parameters are not optimized. In both cases, optimizing parameter values help reach better results. The validity of the proposed model is thus verified for its electrical part, with an error inferior to 2%.

2) Temperature Model: Similarly to the electric model, the temperature model of the cells is compared to measures to verify its validity. Fig. 9 shows the modeled and measured temperature along the test cycle, which is the same as earlier. As both curves are very close to each other and show the same curve shape, the temperature model is also validated with a mean error of 2.45% and a maximal error of 6%.

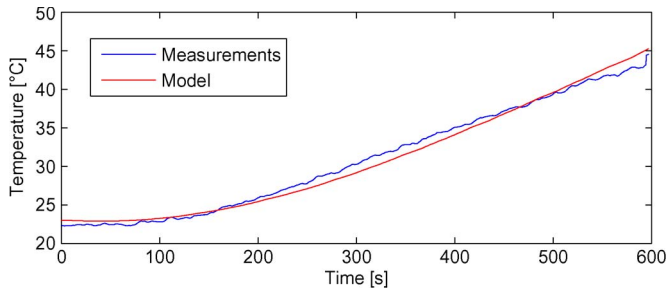

Fig. 9. Comparison of simulation and experimental results for battery temperature.

IV. APPLICATION TO STATE-OF-CHARGE DETERMINATION

Several direct methods have been proposed in the literature [18], [19], based on voltage, electromotive force, OCV [20], or impedance measurements [3], [21], [22].

1) Voltage-based techniques cannot be effectively used on systems such as vehicles, due to the irregular nature of the currents. Moreover, the very flat shape of the OCV curve of $LiFePO_4$ batteries makes this technique very unreliable.
2) Indirect or bookkeeping methods use battery data and current measurements as inputs [3], [23], [24]. The most common one is the Coulomb-counting method, which is an open-loop system, and has the disadvantage of accumulating errors and not correcting them.
3) Adaptive methods such as fuzzy logic [25]–[27], artificial neural networks [28]–[30], and Kalman filters [31], [32] can avoid this issue by combining direct and indirect measurements and automatically adjusting to changing conditions. As lithium-based batteries are strongly affected by external factors and have nonlinear characteristics and behaviors, adaptive systems are a very good fit for an SOC determination algorithm. The Kalman filter method, in its extended form, relies on a battery model belonging to the equivalent circuit model category, and its accuracy therefore depends on the accuracy of the selected equivalent model. This last method is thus selected.

A. Extended Kalman Filters

1) Principle: Kalman filters are algorithms that can be used to minimize measurement noise effects and estimate a system state that cannot be directly measured, such as the SOC of batteries. The filter is a recursive algorithm that combines a model, which is used to estimate a measurable value, and a measurement set. Both values are combined in a weighed average, in which the most weight is given to the value with the least uncertainty. The Kalman filter can then correct the estimation and returns results closer to the true values than the original measurements, as the weighted average has better estimated uncertainty than either of the values that went into the weighted average.

The EKF is an extension of the filter in which the process and measurement equations do not need to be linear, contrary to the classical Kalman filter. A matrix of partial derivatives (Jacobians) is computed and used instead to locally linearize the functions.

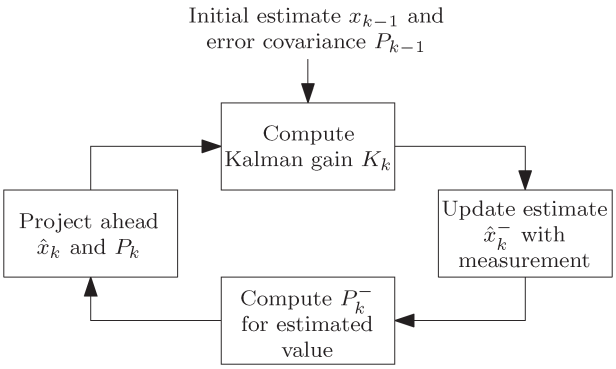

Fig. 10. Simplified flowchart of a Kalman filter.

2) Mathematical Description: The EKF relies on two functions, i.e., a process equation (26), shown below, linking the previous state x_{k-1} to the new state x_k and a measurement equation (27), shown below, i.e.,

$$x_k = f(x_{k-1}, u_{k-1}) + w_{k-1} \tag{26}$$

$$z_k = h(x_k) + v_k. \tag{27}$$

u_k is the measurement, and w_k and v_k are the process and measurement noises.

The filter itself consists of five equations (see Fig. 10): two equations for predicting the measured value, i.e.,

$$\hat{x}_k^- = f(x_{k-1}, u_{k-1}) \tag{28}$$

$$P_k^- = A_{k-1}\, P_{k-1}\, A_{k-1}^T + Q_{k-1} \tag{29}$$

and three equations for correcting it, i.e.,

$$K_k = P_k^-\, H_k^T\, (H_k\, P_k^-\, H_k^T + R_k)^{-1} \tag{30}$$

$$\hat{x}_k = \hat{x}_k^- + K_k\, (z_k - H_k\, \hat{x}_k^-) \tag{31}$$

$$P_k = (I - K_k\, H_k)\, P_k^-. \tag{32}$$

Here, $\hat{V}$ is the estimated value of V, and V^- is the *a priori* value of V.

In these equations, five conditions hold.

1) A_k and H_k are the Jacobian matrices of functions f and h at the current state, i.e.,

$$A_{k-1} = \left.\frac{\partial f}{\partial x}\right|_{x=\hat{x}_{k-1}} \tag{33}$$

$$H_k = \left.\frac{\partial h}{\partial x}\right|_{x=\hat{x}_k}. \tag{34}$$

2) P_k is the *a posteriori* covariance matrix, which is a measure of the estimated accuracy of the state estimate.
3) Q_{k-1} and R_k are the covariances of the process and measurement noises.
4) H_k is the measurement matrix covariance that corrects measurement parameters.
5) K_k is the Kalman filter gain that minimizes the *a posteriori* error covariance.

B. EKF Implementation

For the specific problem of SOC determination, three states are used for the values of the SOC, $V_{\rm st}$, and $V_{\rm lt}$, i.e.,

$$x_k = [\mathrm{SOC}_k; V_{\mathrm{st},k}; V_{\mathrm{lt},k}]. \tag{35}$$

Input u_k is the current measurement, and the filter tries to compare the measured battery voltage $V_{\rm bat}$, with the voltage estimated from the model and the OCV.

Based on (9) and (15), the process and measurement functions (26) and (27) become

$$\hat{x}_k^- = A_{k-1}\, x_{k-1} + B_{k-1}\, I_{k-1} \tag{36}$$

$$A_{k-1} = \begin{pmatrix} 1 & 0 & 0 \\ 0 & e^{\frac{-\Delta t}{R_{\rm st}\, C{\rm st}}} & 0 \\ 0 & 0 & e^{\frac{-\Delta t}{R_{\rm lt}\, C{\rm lt}}} \end{pmatrix}$$

$$B_{k-1} = \begin{pmatrix} \frac{\eta \Delta t}{C_{\rm b}} \\ R_{\rm st}\left(1 - e^{\frac{-\Delta t}{R_{\rm st}\, C{\rm st}}}\right) \\ R_{\rm lt}\left(1 - e^{\frac{-\Delta t}{R_{\rm lt}\, C{\rm lt}}}\right) \end{pmatrix} \tag{38}$$

$$z_k = H_k\, x_k + C_k\, I_k$$

$$H_k = \begin{bmatrix} \frac{\partial \mathrm{OCV}}{\partial \mathrm{SOC}} & -1 & -1 \end{bmatrix}$$

$$C_k = -(R_s + R_{\rm th}). \tag{41}$$

On each iteration of the algorithm, i.e., for each Δt, new measurements for current, battery voltage, and temperature are obtained. The temperature and the last known SOC are used to update the parameters of the model used in the EKF. The filter, which is implemented in Matlab, is then run, updating the value of the SOC through Coulomb-counting and correcting it with a voltage measure.

C. Experimental Results

To validate the accuracy of the algorithm, three different SOC estimation methods are compared. The first method is the EKF, the second method is the Coulomb-counting method, and the third method is a series of discharge tests run under controlled conditions (constant current and temperature). This last method is considered as theoretically the most accurate method to determine a SOC and simply consists of fully discharging the cell to measure its SOC and recharging it by the same amount of energy (while taking charging and discharging efficiencies into account), before going on with the cycle. Several verification points are then obtained through this method and will be used to compare the accuracy of the algorithms.

The selected test profiles consist of a series of three new European driving cycles (NEDC) and a very dynamic racing profile. Unlike in most other experiments in the literature, where cell capacities do not exceed 1.2 Ah and currents 1.2 C, this work uses cells with a much larger capacity, with current profiles ranging from −3 C to 3 C and lasting at least 1 h [19], [24], [28]. The results of these tests are summarized here.

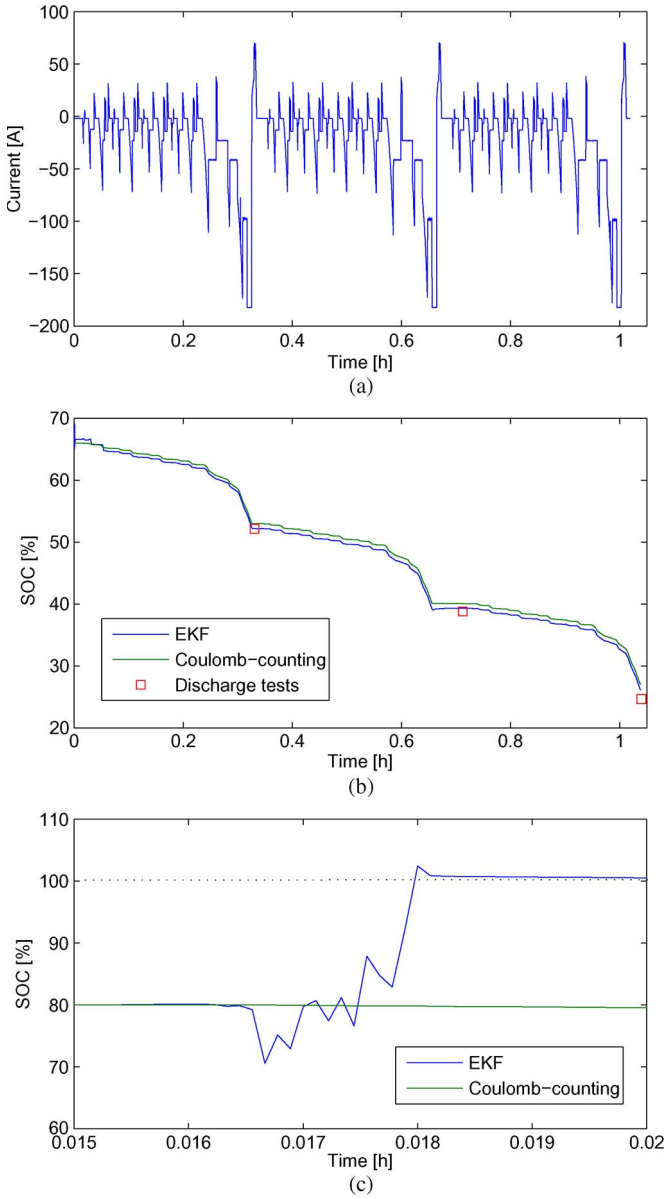

Fig. 11. Comparison of the performance of the three determination methods for the NEDC cycles. (a) Current profile for the three NEDC cycles. (b) Test results with a correct initial SOC for three NEDC cycles. (c) Behavior of both algorithms initialized with an incorrect initial SOC (80%). The real initial SOC is 100%.

A first test is run in Fig. 11, with the first profile consisting of three consecutive NEDC cycles, with a rather slow dynamic [see Fig. 11(a)]. Results shown in Table II and Fig. 11(b) show that the EKF is more precise than the Coulomb-counting method, with a maximum relative error of 6.07% versus 9.57% for the Coulomb-counting method. Similarly, the RMSE, which is given by (42) where N is the number of discharge tests, is of 3.58% for the EKF against 6.00% for the Coulomb-counting method. Table III shows, in detail, the results for the three determination methods, for each test point, and shows that the EKF stays the closest for the values obtained with the discharge tests, i.e.,

$$\mathrm{RMSE}_{\mathrm{EKF}} = \sqrt{\frac{1}{N}\sum_{i=1}^{N}\left(\mathrm{SOC}_{\mathrm{dis}}(i) - \mathrm{SOC}_{\mathrm{EKF}}(i)\right)^2}. \quad (42)$$

TABLE II
RESULTS OF THE COULOMB-COUNTING AND EKF ALGORITHMS COMPARED TO DISCHARGE TEST RESULTS

Test	Figure	Error type	Coulomb-counting	EKF
3 NEDC cycles	Fig. 11(b)	Max. error	9.72 %	6.07 %
3 NEDC cycles	Fig. 11(b)	RMSE	6.00 %	3.58 %
Racing cycle	Fig. 12(b)	Max. error	4.39 %	3.07 %
Racing cycle	Fig. 12(b)	RMSE	3.41 %	1.79 %

TABLE III
SOC RESULTS GIVEN AS A PERCENTAGE OF THE TOTAL CAPACITY FOR THE THREE METHODS FOR THE THREE NEDC CYCLES AT EACH DISCHARGE TEST POINT

Algorithm	Point 1	Point 2	Point 3
Coulomb-counting	53.0	40.1	27.1
EKF	52.2	39.3	26.2
Discharge tests	52.2	38.8	24.7

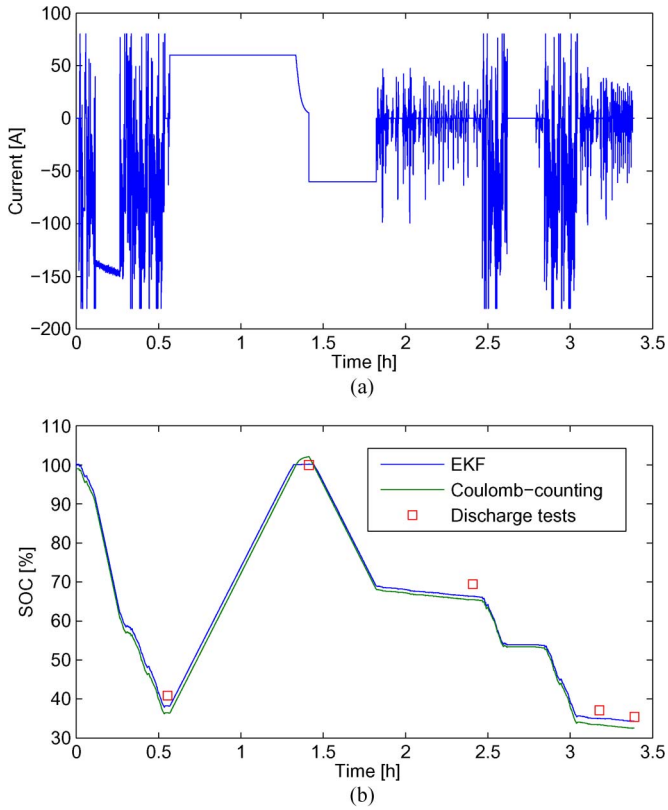

Fig. 12. Comparison of the performance of the three determination methods for the dynamic cycle. (a) Current profile for the racing driving cycle. (b) Comparison of the performance of the three determination methods for the dynamic cycle.

In addition, Fig. 11(c) shows that, contrary to the Coulomb-counting method, the EKF is capable of correcting a wrong initial SOC value. This may happen when the SOC of the battery is not precisely known, e.g., if the battery has been disconnected for a while (and self-discharged) or if it cannot be fully charged before use. In this case, both methods have been initialized with a wrong SOC value of 80%, whereas the real value is 100%. Due to its voltage measurements and model, the EKF manages to quickly converge to values close to the real SOC.

The second test, in Fig. 12, uses a racing driving cycle in which the current profile is very dynamic [see Fig. 12(a)] and shows that the EKF also performs better than the classical

TABLE IV
SOC RESULTS GIVEN AS A PERCENTAGE OF THE TOTAL CAPACITY FOR THE THREE METHODS FOR THE RACING DRIVING CYCLE AT EACH DISCHARGE TEST POINT

Algorithm	Point 1	Point 2	Point 3	Point 4	Point 5
Coulomb-counting	38.3	102.5	73.4	33.4	32.5
EKF	36.5	100.1	72.9	35.7	34.9
Discharge tests	40.9	100.0	69.4	37.1	35.4

current-integration method [see Fig. 12(b)]. This test contains more discharge tests that show the performance of each algorithm at several moments during the test. The maximum error achieved by the Coulomb-counting method is 4.39%, whereas the EKF manages to reduce it to 3.07%. Over the five discharge tests [see Table IV], the RMSE of the EKF is only 1.79%, against 3.41% for the Coulomb-counting method. The EKF is thus also validated with this second more dynamic cycle.

V. CONCLUSION

This paper has presented a multiphysical lithium-based battery pack model with a parameter identification method. An experimental validation has shown that the proposed model performs well, particularly after its parameters have been optimized, also for very dynamic profiles. The application of this model to SOC determination with an EKF has also shown that the combination of both systems has good accuracy, compared to the classical Coulomb-counting method. The proposed elements thus provide a full methodology for characterizing a battery and using it as a SOC determination basis. Future work includes implementing the SOC determination algorithm on an embedded microcontroller and integrating it with a BMS.

ACKNOWLEDGMENT

The authors dedicate this paper to the memory of their friend and coauthor, Dr. B. Blunier, formerly an Associate Professor with the Université de Technologie de Belfort–Montbéliard, who passed away on February 23, 2012.

REFERENCES

[1] M. Urbain, S. Rael, and B. Davat, "Energetical modeling of lithium-ion batteries," in *Conf. Rec. IEEE IAS Annu. Meeting*, 2007, pp. 714–721.
[2] S. Pang, J. Farrell, J. Du, and M. Barth, "Battery state-of-charge estimation," in *Proc. Amer. Control Conf.*, 2001, vol. 2, pp. 1644–1649.
[3] V. Pop, H. J. Bergveld, D. Danilov, P. P. L. Regtien, and P. H. L. Notten, *Battery Management Systems, Accurate State-of-Charge Indication for Battery-Powered Applications*. New York: Springer-Verlag, 2008.
[4] V. Spath, A. Jossen, H. Doring, and J. Garche, "The detection of the state of health of lead-acid batteries," in *Proc. 19th INTELEC*, 1997, pp. 681–686.
[5] M. Dubarry, V. Svoboda, R. Hwu, and B. Liaw, "Capacity loss in rechargeable lithium cells during cycle life testing: The importance of determining state-of-charge," *J. Power Sources*, vol. 174, no. 2, pp. 1121–1125, 2007.
[6] F. Conte, "Battery and battery management for hybrid electric vehicles: A review," *e & i Elektrotechnik und Informationstechnik*, vol. 123, no. 10, pp. 424–431, Oct. 2006.
[7] P. Sinclair, R. Duke, and S. Round, "An adaptive battery monitoring system for an electric vehicle," in *Proc. Int. Conf. Power Electron. Drives Energy Syst. Ind. Growth*, 1998, vol. 2, pp. 786–791.
[8] A. Capel, "Mathematical model for the representation of the electrical behaviour of a lithium cell," in *Proc. IEEE Power Electron. Spec. Conf.*, 2001, vol. 4, pp. 1976–1981.
[9] R. C. Kroeze and P. T. Krein, "Electrical battery model for use in dynamic electric vehicle simulations," in *Proc. IEEE Power Electron. Spec. Conf.*, 2008, pp. 1336–1342.
[10] J. Larminie and J. Lowry, *Electric Vehicle Technology Explained*. Hoboken, NJ: Wiley, 2003.
[11] N. A. Chaturvedi, R. Klein, J. Christensen, J. Ahmed, and A. Kojic, "Algorithms for advanced battery-management systems," *IEEE Control Syst. Mag.*, vol. 30, no. 3, pp. 49–68, Jun. 2010.
[12] C. Min and G. Ricon-Mora, "Accurate electrical battery model capable of predicting runtime and I– V performance," *IEEE Trans. Energy Convers.*, vol. 21, no. 2, pp. 504–511, Jun. 2006.
[13] S. Chen, K. Tseng, and S. Choi, "Modeling of lithium-ion battery for energy storage system simulation," in *Proc. Power Energy Eng. Conf.*, 2009, vol. 21, pp. 1–4.
[14] J. Van Mierlo, P. Van den Bossche, and G. Maggetto, "Models of energy sources for EV and HEV: Fuel cells, batteries, ultracapacitors, flywheels and engine-generators," *J. Power Sources*, vol. 128, no. 1, pp. 76–89, Mar. 2004.
[15] B. Schweighofer, K. M. Raab, and G. Brasseur, "Modeling of high power automotive batteries by the use of an automated test system," *IEEE Trans. Instrum. Meas.*, vol. 52, no. 4, pp. 1087–1091, Aug. 2003.
[16] S. Abu-Sharkh and D. Doerffel, "Rapid test and non-linear model characterisation of solid-state lithium-ion batteries," *J. Power Sources*, vol. 130, no. 1/2, pp. 266–274, 2004.
[17] M. Wright, *An Introduction to Chemical Kinetics*. Hoboken, NJ: Wiley, 2004.
[18] V. Prajapati, H. Hess, E. William, V. Gupta, M. Huff, M. Manic, F. Rufus, A. Thakker, and J. Govar, "A literature review of state-of-charge estimation techniques applicable to lithium poly-carbon monoflouride (LI/CFx) battery," in *Proc. IICPE*, pp. 1–8.
[19] M. Coleman, C. Lee, C. Zhu, and W. Hurley, "State-of-charge determination from EMF voltage estimation: Using impedance, terminal voltage, and current for lead-acid and lithium-ion batteries," *IEEE Trans. Ind. Electron.*, vol. 54, no. 5, pp. 2550–2557, Oct. 2007.
[20] D. Cadar, D. Petreus, and C. Orian, "A method of determining a lithium-ion battery's state of charge," in *Proc. 15th SIITME*, 2009, pp. 257–260.
[21] S. Rodrigues, N. Munichandraiah, and A. Shukla, "A review of state-of-charge indication of batteries by means of ac impedance measurements," *J. Power Sources*, vol. 87, no. 1/2, pp. 12–20, 2000.
[22] F. Huet, "A review of impedance measurements for determination of the state-of-charge or state-of-health of secondary batteries," *J. Power Sources*, vol. 70, no. 1, pp. 59–69, 1998.
[23] S. Piller, M. Perrin, and A. Jossen, "Methods for state-of-charge determination and their applications," *J. Power Sources*, vol. 96, no. 1, pp. 113–120, Jun. 2001.
[24] K. Ng, C. Moo, Y. Chen, and Y. Hsieh, "Enhanced Coulomb counting method for estimating state-of-charge and state-of-health of lithium-ion batteries," *Appl. Energy*, vol. 86, no. 9, pp. 1506–1511, 2009.
[25] X. Hu and F. Sun, "Fuzzy clustering based multi-model support vector regression state of charge estimator for lithium-ion battery of electric vehicle," in *Proc. Int. Conf. Intell. Hum.-Mach. Syst. Cybern.*, 2009, pp. 392–396.
[26] A. Zenati, P. Desprez, and H. Razik, "Estimation of the SOC and the SOH of Li-ion batteries, by combining impedance measurements with the fuzzy logic inference," in *Proc. 36th IEEE IECON*, 2010, pp. 1773–1778.
[27] A. Zenati, P. Desprez, H. Razik, and S. Rael, "Impedance measurements combined with the fuzzy logic methodology to assess the soc and soh of lithium-ion cells," in *Proc. IEEE VPPC*, 2010, pp. 1–6.
[28] M. Charkhgard and M. Farrokhi, "State-of-charge estimation for lithium-ion batteries using neural networks and EKF," *IEEE Trans. Ind. Electron.*, vol. 57, no. 12, pp. 4178–4187, Dec. 2010.
[29] S. Grewal and D. Grant, "A novel technique for modelling the state of charge of lithium ion batteries using artificial neural networks," in *Proc. 23rd INTELEC*, 2001, pp. 174–179.
[30] W. He, D. Huang, and D. Feng, "The prediction of SOC of lithium batteries and varied pulse charge," in *Proc. ICMA*, 2009, pp. 1578–1582.
[31] F. Sun, X. Hu, Y. Zou, and S. Li, "Adaptive unscented Kalman filtering for state of charge estimation of a lithium-ion battery for electric vehicles," *Energy*, vol. 36, no. 5, pp. 3531–3540, May 2011.
[32] H. He, R. Xiong, X. Zhang, F. Sun, and J. Fan, "State-of-charge estimation of lithium-ion battery using an adaptive extended Kalman filter based on an improved Thevenin model," *IEEE Trans. Veh. Technol.*, vol. 60, no. 4, pp. 1461–1469, May 2011.

Nicolas Watrin (S'10) received the M.S. degree in electrical engineering in 2009 from the Université de Technologie de Belfort–Montbéliard, Belfort, France, where he is currently working toward the Ph.D. degree in association with Segula Technologie Automotive, Villeneuve d'Ascq, France.

His current research interests include multiphysical hybrid vehicle modeling and hybrid system sizing.

Robin Roche (S'09) received the M.S. degree in electrical engineering in 2009 from the Université de Technologie de Belfort–Montbéliard, Belfort, France, where he is currently working toward the Ph.D. degree in electrical engineering with the Research Institute on Transportation, Energy and Society.

His research interests include intelligent energy management in power systems, smart grids, applications of computational intelligence, energy storage and hybrid vehicles, and the societal and economic impacts of these technologies.

Hugues Ostermann received the M.S. degree in electrical engineering from the Université de Technologie de Belfort–Montbéliard (UTBM), Belfort, France, in 2004.

From 2005 to 2009, he was an Electrical Maintenance Engineer in the heavy process industry and a PLC Software Developer for industrial process control. Since 2009, he has been involved in teaching and research activities with the Research Institute on Transportation, Energy and Society, UTBM. His research interests include hybrid powertrains and embedded energy storage.

Benjamin Blunier received the M.Sc. and Ph.D. degrees in electrical engineering from the Université de Technologie de Belfort–Montbéliard (UTBM), Belfort, France, in 2004 and 2007, respectively.

He studied fuel cell system modeling and, particularly, their air management and control for hybrid and electric vehicles. He was an Associate Professor with the Research Institute on Transportation, Energy and Society, UTBM, until his death on February 23, 2012. His research interests included fuel cells systems; electric, hybrid and plug-in hybrid vehicles; and intelligent energy management in smart grids and microgrids.

Abdellatif Miraoui (SM'09) was born in Morocco, in 1962. He received the M.Sc. degree from Haute Alsace University, Mulhouse, France, in 1988 and the Ph.D. and Habilitation degrees from the University of Franche-Comté, Besancon, France, in 1992 and 1999, respectively.

He is currently the President of Cadi Ayyad University, Marrakesh, Morocco. Since 2000, he has been a Full Professor of electrical engineering (electrical machines and energy) with the Université de Technologie de Belfort–Montbéliard, Belfort, France, where he was the Vice President of Research Affairs from 2008 to 2011, the Director of the Electrical Engineering Department from 2001 to 2009, and the Head of the "Energy Conversion and Command" Research Team (38 researchers in 2007). He is the author of more than 80 journal and 150 international conference proceeding papers and four textbooks about fuel cells. His research interests include fuel cell energy, energy management in transportation, and design and optimization of electrical propulsions/tractions.

Dr. Miraoui is a Doctor Honoris Causa of the Technical University of Cluj-Napoca, Cluj-Napoca, Romania. He was an Editor of the *International Journal on Electrical Engineering Transportation*. He is a member of several international journal and conference committees. He is a member of the IEEE Power Electronics, IEEE Industrial Electronics, and IEEE Vehicular Technology Societies. He received a high distinction from the French Higher Education Ministry "Chevalier dans l'Ordre des Palmes Académiques" in 2007. He was also distinguished as an Honorary Professor by the Transylvania University of Brasov, Brasov, Romania.